© 2020. Published by The Company of Biologists Ltd | Development (2020) 147, dev189902. doi:10.1242/dev.189902

RESEARCH ARTICLE

The RALF1-FERONIA interaction modulates endocytosis to mediate control of root growth in *Arabidopsis*

Meng Yu[1,2,*], Ruili Li[1,2,*], Yaning Cui[1,2], Weijun Chen[3], Bin Li[3], Xi Zhang[2], Yufen Bu[2], Yangyang Cao[2], Jingjing Xing[4], Pawan Kumar Jewaria[1], Xiaojuan Li[1,2], Rishikesh P. Bhalerao[1,5], Feng Yu[3,‡] and Jinxing Lin[1,2,‡]

ABSTRACT

The interaction between the receptor-like kinase (RLK) FERONIA (FER) and the secreted peptide RAPID ALKALINIZATION FACTOR1 (RALF1) is vital for development and stress responses in *Arabidopsis*. Ligand-induced membrane dynamics affect the function of several RLKs, but the effects of the RALF1-FER interaction on the dynamics of FER and the ensuing effects on its functionality are poorly understood. Here, we show that RALF1 modulated the dynamics and partitioning of FER-GFP at the plasma membrane (PM). Moreover, FER was internalized by both clathrin-mediated endocytosis (CME) and clathrin-independent endocytosis (CIE) under steady-state conditions. After RALF1 treatment, FER-GFP internalization was primarily enhanced via the CME pathway, raising FER-GFP levels in the vacuole. RALF1 treatment also modulated trafficking of other PM proteins, such as PIN2-GFP and BRI1-GFP, increasing their vacuolar levels by enhancing their internalization. Importantly, blocking CME attenuated RALF1-mediated root growth inhibition independently of RALF1-induced early signaling, suggesting that the RALF1 can also exert its effects via the CME pathway. These findings reveal that the RALF1-FER interaction modulates plant growth and development, and this might also involve endocytosis of PM proteins.

KEY WORDS: RALF1, FERONIA, Endocytosis, Root growth, *Arabidopsis*

INTRODUCTION

Receptor-like kinases (RLKs) play crucial roles in plant development by perceiving changes in the cellular environment through their distinct extracellular domains, which are used to categorize the RLKs into different superfamilies. The *Catharanthus roseus* RLK1-like kinase (CrRLK1L) subfamily in *Arabidopsis thaliana* consists of 17 members with a putative extracellular carbohydrate-binding malectin-like domain (Schulze-Muth et al., 1996; Boisson-Dernier et al., 2011; Nissen et al., 2016). Recent studies have shown that several CrRLK1Ls are key modulators of cell elongation and are also involved in sexual reproduction (Lindner et al., 2012; Nissen et al., 2016; Liao et al., 2017). For example, THESEUS1 (THE1) and HERCULES1 (HERK1) are putative cell wall integrity sensors, with the double CrRLK1L mutant *the1herk1* exhibiting inhibited root cell elongation (Guo et al., 2009). The other two CrRLK1Ls, BUDDHAS PAPER SEAL1 (BUPS1) and BUDDHAS PAPER SEAL2 (BUPS2), can interact with ANXUR1 and ANXUR2 to control pollen tube rupture (Ge et al., 2017).

FER is one of the most extensively studied CrRLK1Ls and was originally identified as a key factor in pollen tube reception, contributing to fertilization in *Arabidopsis* (Huck et al., 2003; Kessler et al., 2010). FER is also involved in several other important biological processes, including hormone signaling, cell elongation and pathogen defense (Duan et al., 2010; Yu et al., 2012; Stegmann et al., 2017). Haruta et al. (2014) showed that a secreted peptide, RAPID ALKALINIZATION FACTOR1 (RALF1), can specifically bind as a ligand to the extracellular domain of FER (Haruta et al., 2014). Moreover, RALF1 treatment induced the phosphorylation of the plasma membrane (PM) H^+-ATPase AHA2 at Ser899, which might result in reduced primary root elongation (Haruta et al., 2014). A receptor-like cytoplasmic kinase, RPM1-INDUCED PROTEIN KINASE (RIPK), was recently identified as an interacting partner of FER, making it a downstream factor in RALF1-induced signal transduction (Du et al., 2016). Another recent study showed that RALF1 can interact directly with the extracellular domain of BRI1-ASSOCIATED RECEPTOR KINASE1 (BAK1) to enhance its phosphorylation. However, although RALF1 induced apoplastic alkalinization in the *bak1* mutant, this did not cause inhibition of root elongation in these plants (Dressano et al., 2017). Therefore, the precise mechanism of RALF1-FER mediated inhibition of root elongation is complex and far from clear.

In plants, several studies have shown that RLK levels at the PM are dynamically controlled by protein trafficking. Endocytosis can not only decrease RLK intensity at the PM, thereby attenuating signaling, but can also contribute to downstream signal transduction in the endosomes. For example, the clathrin-mediated endocytosis (CME) is important for FLAGELLIN SENSING 2- (FLS2, a classical pattern recognition receptor) dependent induction of callose deposition and stomatal closure but not MAPK activation (Mbengue et al., 2016). Moreover, the levels of PM-localized proteins at the PM have important effects on their function. For example, reduced BRI1 exocytosis in the *det3* mutation of subunit C of the vacuolar H^+-ATPase (V-ATPase) causes attenuation of brassinosteroid-induced signal transduction (Luo et al., 2015).

To our knowledge, most previous studies on FER have focused on the initiation of its signaling pathway and its transduction from the PM. However, little is known about the endocytic pathways and trafficking routes of FER, or their effects on FER-mediated control

[1]Beijing Advanced Innovation Center for Tree Breeding by Molecular Design, Beijing Forestry University, Beijing 100083, China. [2]College of Biological Sciences and Technology, Beijing Forestry University, Beijing 100083, China. [3]College of Biology, Hunan Key Laboratory of Plant Functional Genomics and Developmental Regulation, Hunan University, Changsha 410082, China. [4]State Key Laboratory of Crop Stress Adaptation and Improvement, School of Life Sciences, Henan University, Kaifeng 475001, China. [5]Umeå Plant Science Centre, Department of Forest Genetics and Plant Physiology, Swedish University of Agricultural Sciences, S-901 83 Umeå, Sweden.
*These authors contributed equally to this work

‡Authors for correspondence (linjx@ibcas.ac.cn; feng_yu@hnu.edu.cn)

M.Y., 0000-0002-5221-281X; X.Z., 0000-0001-5518-4220; P.K.J., 0000-0002-1961-3750; J.L., 0000-0001-9338-1356

Handling Editor: Ykä Helariutta
Received 26 February 2020; Accepted 2 June 2020

Development (2020) 147, dev189902. doi:10.1242/dev.189902

of plant development. Therefore, this work explores the dynamics and partitioning of FER-GFP at the PM and inside the cell using live-cell imaging. We also explored the effect of the RALF1-FER interaction on FER trafficking. Our results show that RALF1 enhanced the internalization of FER and that the RALF1-FER interaction was also important for the internalization and trafficking of other PM-localized proteins. Moreover, impairment of CME attenuated RALF1-induced root growth inhibition. Taken together, our results indicated that the modulation of plant development by the RALF1-FER interaction might also be mediated by its effects on the endocytosis and trafficking of PM proteins.

RESULTS

The dynamics and oligomeric state of FER-GFP at the PM

To investigate the dynamics of FER, we used confocal microscopy to visualize the FER-GFP fusion protein expressed under the control of the native *FER* promoter in the *fer-4* (a FER null mutant) background. FER-GFP was primarily observed at the PM, as reported previously (Duan et al., 2010), but was also present at intracellular punctate structures in the *Arabidopsis* root (Fig. S1). To visualize the state of FER-GFP at the PM, we monitored the dynamics of FER-GFP in epidermal cells using variable-angle total internal reflection fluorescence microscopy (VA-TIRFM), which provides high-resolution and high signal-to-noise ratio images. The FER-GFP fluorescence formed discrete and diffraction-limited spots that displayed high-speed dynamics at the PM (Fig. 1A,B). Moreover, some FER-GFP spots disappeared from the PM after a long period of residence, whereas other spots appeared to rise up from within the cell (Fig. 1B). In order to evaluate the diffusion types of FER-GFP at the PM, we analyzed the mean square displacement (MSD) versus time plots of the trajectories of individual molecules, which reflected the diffusion types of molecules (Li et al., 2011). The type of the curve-fitting relationship between MSD and time revealed that FER-GFP exhibited four diffusion modes: simple Brownian diffusion; restricted diffusion limited by corrals or impaired by obstacles; high velocity directed diffusion; and mixed diffusion combining Brownian and restricted modes (Fig. S2).

We also analyzed the dynamics of FER-GFP based on their trajectories, which were obtained by VA-TIRFM. Based on motion range (distance traveled), FER-GFP was classified into two subpopulations: short distance (22.0% of all observed movements, mean movement length 0.255±0.006 µm) and long distance (78.0%, 0.573±0.022 µm) (Fig. 1C,E). After treatment with the FER ligand RALF1, the relative frequency of short-distance motion range increased to 34%, whereas their mean length fell to 0.217±0.004 µm; the relative frequency of long-distance motion range fell to 66.0% and their mean length fell to 0.535±0.030 µm (Fig. 1D,E). RALF1 treatment thus restricted FER-GFP to a smaller area. We also analyzed the diffusion coefficients of FER-GFP, plotted histograms of their distribution and fitted them to a Gaussian function (Gaussian peaks are denoted $\hat{G}$) and the $\hat{G}$ were considered as the characteristic diffusion coefficients. RALF1 treatment reduced the diffusion coefficient of FER-GFP from 1.8047±0.2612×10^{-2} µm/s^2 to 1.0366±0.2079×10^{-2} µm/s^2 (Fig. 1F-H), indicating that RALF1 treatment reduced the diffusion of FER-GFP within the PM. Previous studies showed that the formation of microdomains can restrict the dynamics of PM proteins (Douglass

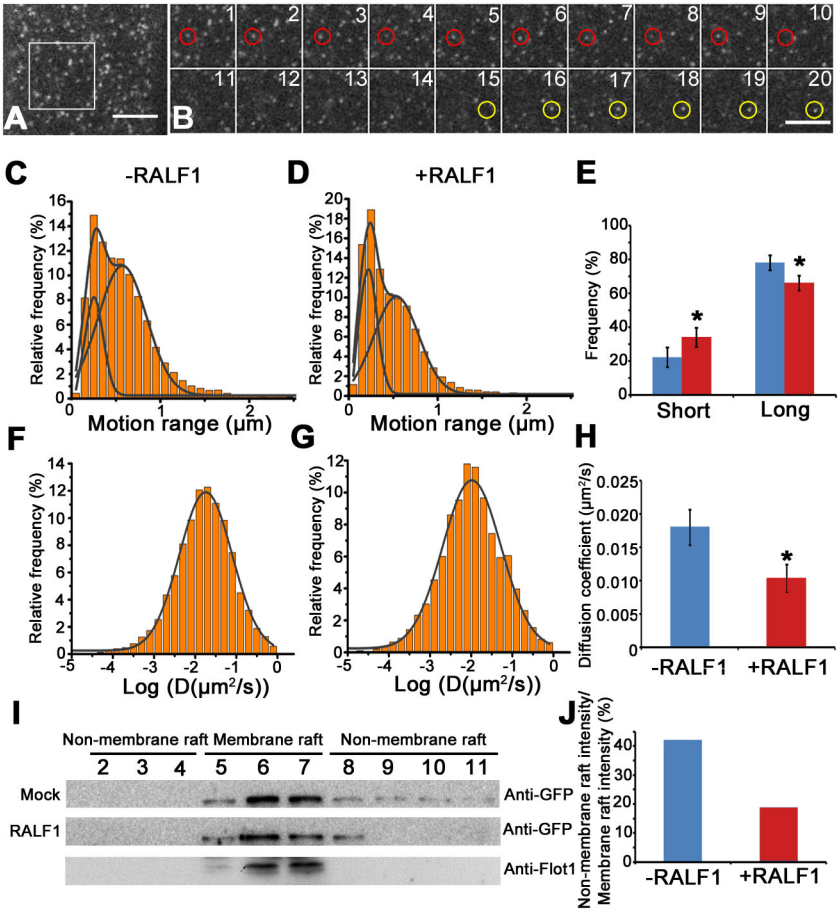

Fig. 1. Dynamic behaviors and partitioning of FER-GFP at the PM in *Arabidopsis* seedlings. (A) A single-particle VA-TIRFM image of FER-GFP at the PM in *Arabidopsis* root cells. (B) A time series of images of the boxed area in A. Red and yellow circles indicate the disappearance and appearance of FER-GFP particles at the PM, respectively. (C) Distribution of FER-GFP motion range in living root cells (*n*=17,167 spots). (D) Distribution of FER-GFP motion range in living root cells treated with RALF1 (*n*=19,358 spots). (E) Comparison of FER-GFP motion range in living root cells with (red) and without (blue) RALF1 treatment. (F) Distribution of FER-GFP diffusion coefficients in living root cells (*n*=3815 spots). (G) Distribution of FER-GFP diffusion coefficients in living root cells after treatment with RALF1 (*n*=3858 spots). (H) Comparison of FER-GFP diffusion coefficients in living root cells with or without RALF1 treatment. (I) The partitioning of FER-GFP between membrane rafts and non-raft sections of the plasma membrane with or without RALF1 treatment. (J) Intensity of FER-GFP fluorescence in membrane rafts and non-membrane rafts. *P<0.05 (paired two-tailed Student's *t*-test). Data are mean±s.d. Scale bars: 10 µm.

Development (2020) 147, dev189902. doi:10.1242/dev.189902

and Vale, 2005). Therefore, we speculated that RALF1 treatment might induce FER-GFP enrichment in microdomains. To test this hypothesis, we analyzed the partitioning of FER-GFP between membrane rafts and non-rafts by sucrose gradient ultracentrifugation, revealing that RALF1 treatment induced extensive FER-GFP enrichment in membrane rafts (Fig. 1I,J).

We next analyzed the homo-oligomeric state of FER-GFP at the PM using VA-TIRFM combined with progressive idealization and filtering (PIF) algorithms (McGuire et al., 2012). This revealed that FER-GFP at the PM exhibited both one-step and two-step photobleaching (Fig. 2A,B), indicating that FER exists as a monomer or homodimer. Of the FER-GFP molecules, 8.2% exhibited two-step photobleaching, whereas 91.8% showed one-step photobleaching (Fig. 2C), indicating that FER-GFP mainly existed as a monomer under normal growth conditions. After RALF1 treatment, 8% of FER-GFP molecules exhibited two-step photobleaching, whereas 92% showed one-step photobleaching (Fig. 2C), indicating that the majority of FER-GFP proteins remained as monomers at the PM in the presence of RALF1. We also performed a bimolecular fluorescence complementation (BiFC) assay in a tobacco (*Nicotiana tabacum*) expression system to verify that FER mainly existed as a monomer at the PM (Cui et al., 2019). Mao et al. (2015) have shown that FER can interact with S-ADENOSYLMETHIONINE SYNTHETASE 1 (SAM1) at the PM (Mao et al., 2015). Our results showed that YFP fluorescence was observed in tobacco leaves co-expressing *FER-nYFP* and *SAM1-cYFP* as controls but not in leaves co-expressing *FER-nYFP* and *FER-cYFP* with or without RALF1 (Fig. 2D). In combination with photobleaching step experimental results, all the data suggest that FER is primarily monomeric at the PM, independently of RALF1 treatment.

The subcellular localization and trafficking of FER under steady-state conditions

We next investigated the intracellular localization of FER. After a 30 min treatment with FM4-64, a lipophilic styryl dye used to stain the PM and trace endocytosis, we found that intracellular FER-GFP fluorescence was mainly colocalized with the FM4-64 label in *Arabidopsis* roots (Fig. 3A). As FM4-64 can label endosomes within this timeframe, FER-GFP appears to reside at the endosomes in addition to the PM. To identify other FER-GFP-positive intracellular compartments, we also analyzed the colocalization of FER-GFP with fluorescence-tagged endomembrane markers. FER-GFP colocalized mainly (87.8%) with the trans-Golgi network (TGN) marker VHA-a1-mRFP (Fig. 3B). Conversely, only 8.4% of FER-GFP colocalized with the Golgi marker MEMB12-mCherry (Fig. 3C), whereas 9.2% of FER-GFP was associated with the multivesicular body (MVB) marker ARA7-RFP (Fig. 3D).

We then investigated FER trafficking using the fungal toxin brefeldin A (BFA), which is an inhibitor of ARF-GEF-type vesicle transport regulators (Nebenfuhr et al., 2002; Ritzenthaler et al., 2002; Tse et al., 2007). Following BFA treatment, FER-GFP mainly accumulated in BFA compartments together with FM4-64. This localization was unaffected by treatment with cycloheximide (CHX), an inhibitor of protein biosynthesis (Fig. 3E, Fig. S3A). These observations were confirmed by the finding that pretreatment with CHX for 1 h and then treatment with BFA and CHX together, resulted in FER-GFP colocalization with VHA-a1-RFP in the BFA compartments (Fig. 3F, Fig. S3B). Overall, these results suggest that the internalized FER-GFP will be transported to the TGN under steady-state conditions.

It has been reported that several proteins can also be sorted to the vacuole after cellular internalization from the PM (Claus et al., 2018). To determine whether FER-GFP was also sorted to the vacuole, we analyzed FER-GFP localization after treatment with concanamycin A (Conc A). Conc A inhibits protein degradation in the vacuole by inhibiting the activity of vacuolar H^+-ATPase (Páli et al., 2004). After Conc A treatment in the light, weak FER-GFP fluorescence was observed in the vacuoles (Fig. 3G), indicating that FER-GFP was indeed sorted to the vacuole.

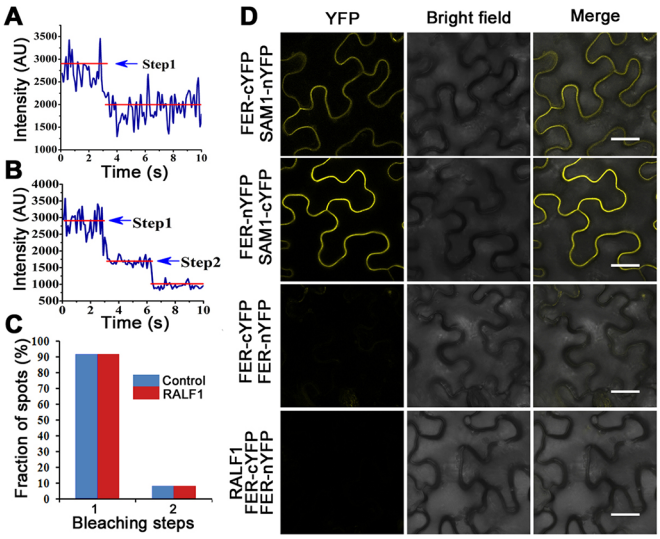

Fig. 2. The oligomeric status of FER-GFP at the PM of living cells. (A) Time-course of GFP emissions after background correction showing one-step photobleaching. (B) Time-course of GFP emissions after background correction showing two-step photobleaching. (C) Distribution of FER-GFP photobleaching steps with (red, *n*=573) and without (blue, *n*=548) RALF1 treatment. (D) BiFC analysis of FER interacting with itself with or without RALF1 treatment. AU, arbitrary units. Scale bars: 20 µm.

FER was internalized via clathrin-dependent and -independent pathways

Both CME and clathrin-independent endocytosis (CIE) have previously been reported in *Arabidopsis* (Fan et al., 2015), prompting us to investigate the endocytic pathways by which FER-GFP is internalized. As shown in Fig. 4A, the ratios of FER-GFP signals between the cytosol and PM were significantly lower in CME-defective clathrin light chain (CLC) *clc2-1/3-1* and CME-defective clathrin heavy chain (CHC) *chc2-1* mutant roots than in control seedlings, indicating that some FER-GFP internalization occurs by CME (Fig. 4A). CIE is another important pathway for the internalization of PM proteins that relies on sterols (Li et al., 2011). We therefore investigated the role of CIE in FER-GFP endocytosis by analyzing FER trafficking in the presence of the sterol-depleting agent methyl-β-cyclodextrin (MβCD), which can affect the CIE pathway (Li et al., 2011; Wang et al., 2013b; Hao et al., 2014; Fan et al., 2015). MβCD treatment significantly reduced the ratio of FER-GFP signal strength in the cytosol and PM relative to that seen in control seedlings (Fig. 4B), implying that CIE also contributed to FER-GFP internalization under steady-state conditions. Flot1 is involved in a CIE pathway and has been popularly used to study the clathrin-independent pathway (Li et al., 2011, 2012; Yu et al., 2017). Therefore, to directly confirm that FER-GFP is internalized by both CME and CIE, we analyzed the colocalization of FER-GFP with the CME marker protein CLC-mCherry and the CIE marker protein Flot1-mCherry at the PM using VA-TIRFM. FER-GFP colocalization with both CLC-mCherry (Fig. 4C) and Flot-mCherry

Development (2020) 147, dev189902. doi:10.1242/dev.189902

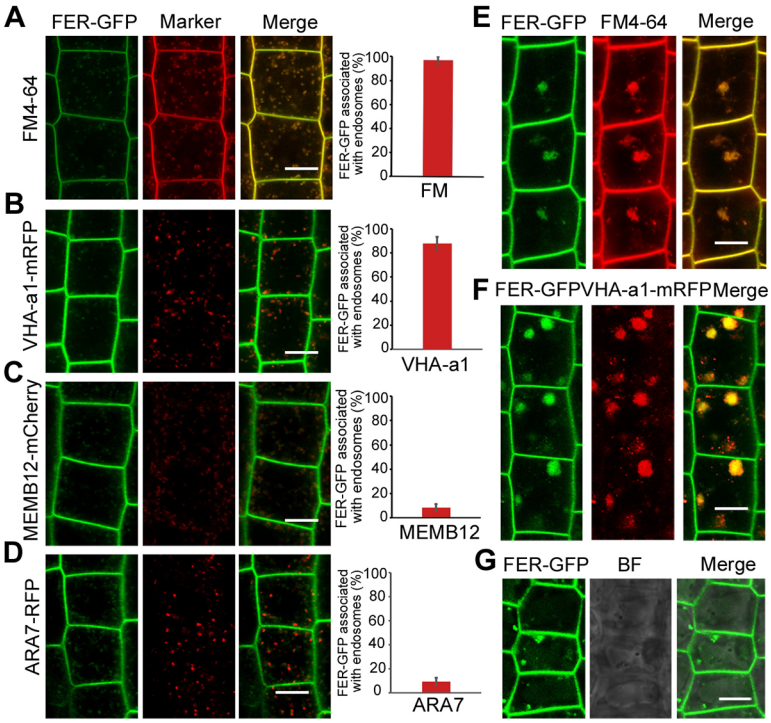

Fig. 3. The intracellular trafficking of FER-GFP in a steady-state condition. (A) Colocalization of FER-GFP with FM4-64 after FM4-64 staining for 30 min. *n*=392 compartments. (B-D) Colocalization of FER-GFP with the TGN marker protein VHA-a1-mRFP, the Golgi marker protein MEMB12-mCherry and the late endosome marker protein ARA7-RFP. *n*=328, 428 and 392 compartments, respectively. (E) FER-GFP colocalization with FM4-64 in the BFA compartment. The seedling roots were pretreated with CHX for 1 h and then incubated with BFA and CHX for 45 min. FM4-64 was then added for another 15 min incubation. (F) FER-GFP colocalization with the TGN marker protein VHA-a1-mRFP in the BFA compartment. The roots of the seedlings were pretreated with CHX for 1 h and then incubated with BFA and CHX for 1 h. (G) FER-GFP accumulation in the vacuole after treatment with Conc A for 6 h. FM4-64, 5 µM; BFA, 50 µM; CHX, 50 µM; Conc A, 2 µM. BF, bright field. Data are mean±s.d. Scale bars: 10 µm.

(Fig. 4D) was detected at the PM, demonstrating that FER-GFP was indeed internalized by both CME and CIE.

RALF1 promoted FER-GFP internalization that required CME

We next investigated whether RALF1, the specific ligand of FER, can modulate the intracellular trafficking pathway of FER-GFP, as signaling via RLKs often relies on ligand-mediated trafficking (Claus et al., 2018). RALF1 treatment enhanced the accumulation of FER-GFP inside the cell (Fig. 5A) and caused the accumulated FER-GFP to colocalize with FM4-64, indicating that it was localized to the endosomes (Fig. 5B). FER-GFP also colocalized with the TGN marker protein VHA-a1-RFP after RALF1 treatment

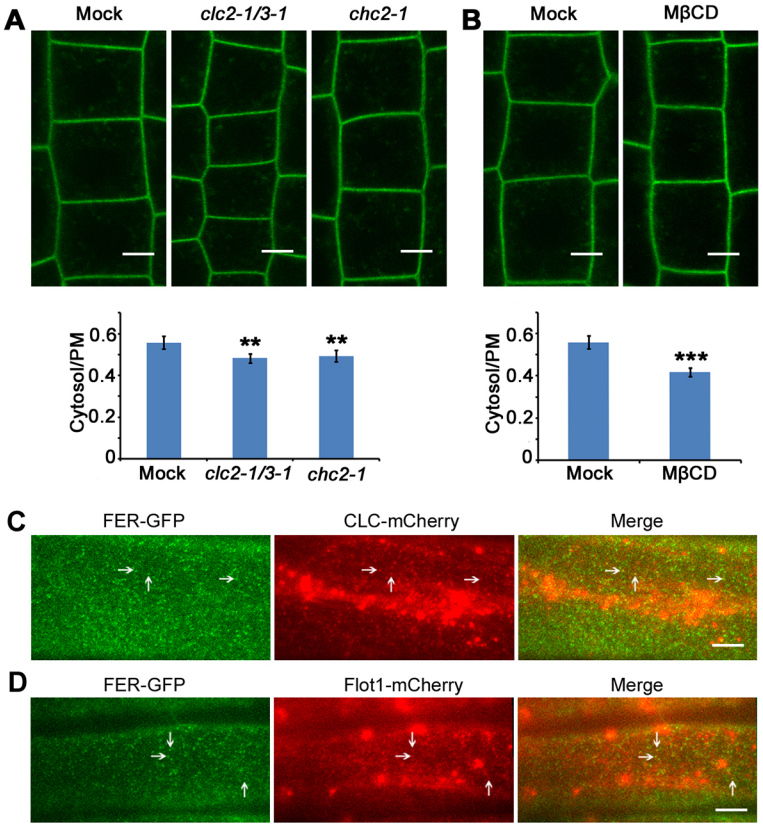

Fig. 4. FER-GFP internalization is mediated by CME and CIE. (A) The ratios of FER-GFP signal intensity in the cytosol and PM in the roots of wild-type seedlings and CME-defective *clc2-1/3-1* and *chc2-1* mutant seedlings. *n*=27, 27 and 27 cells, respectively. Scale bars: 10 µm. (B) Ratios of FER-GFP signal intensity between the cytosol and PM in control roots and MβCD-treated roots. *n*=30 and 30 cells, respectively. Scale bars: 10 µm. (C) VA-TIRFM revealed that some FER-GFP molecules colocalized with CLC-mCherry at the PM. Scale bar: 5 µm. (D) VA-TIRFM revealed that some FER-GFP molecules colocalized with Flot1-mCherry at the PM. Scale bar: 5 µm. ***P*<0.01, ****P*<0.001 (paired two-tailed Student's *t*-test). Data are mean±s.d.

Development (2020) 147, dev189902. doi:10.1242/dev.189902

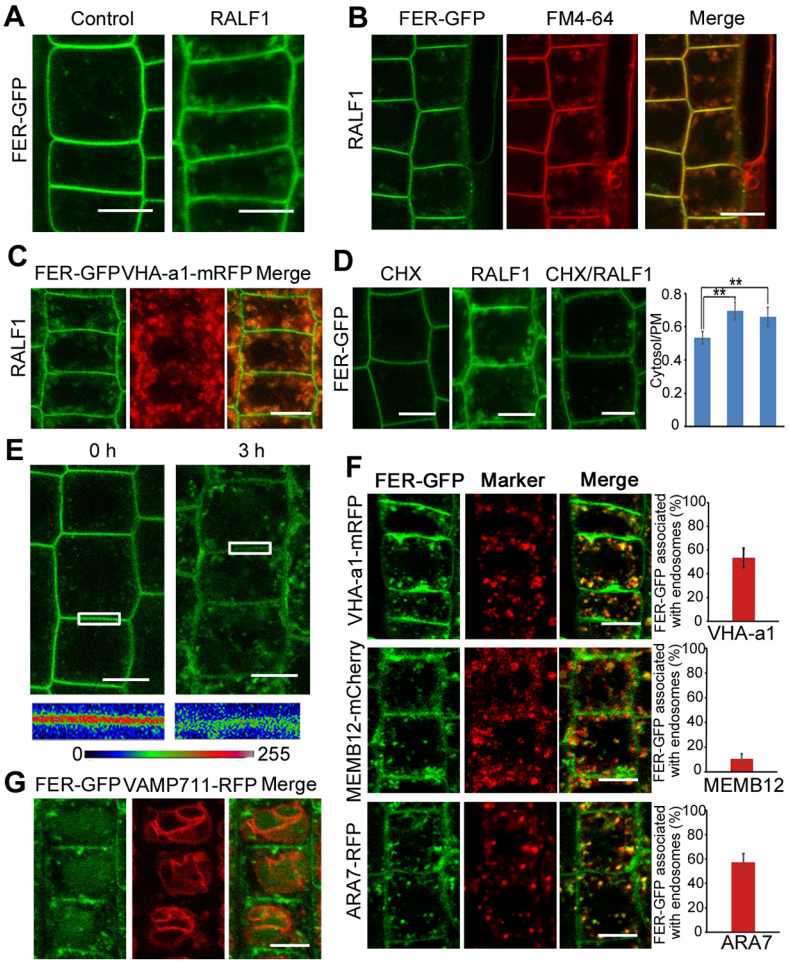

Fig. 5. RALF1 treatment enhanced the internalization of FER-GFP to the vacuole. (A) FER-GFP accumulation inside the cell after a 1 h RALF1 treatment. (B) FER-GFP colocalization with FM4-64 inside the cell after a 1 h RALF1 treatment. (C) FER-GFP colocalization with the TGN marker VHA-a1-RFP inside the cell after a 1 h RALF1 treatment. (D) The ratios of FER-GFP signal intensity in the cytosol and PM in the cells after CHX pretreatment for 1 h followed by a 1 h treatment with RALF1 and CHX. *n*=21, 21 and 18 cells, respectively. (E) The fluorescence of FER-GFP at the PM after a 3 h RALF1 treatment. Pseudocolor images (blue-yellow-red palette) showing the fluorescence intensity of FER-GFP in the boxed areas. (F) The colocalization of FER-GFP with TGN marker protein VHA-a1-mRFP, Golgi marker protein MEMB12-mCherry and late endosome marker protein ARA7-RFP after RALF1 treatment for 3 h. *n*=417, 439 and 419 compartments, respectively. (G) FER-GFP accumulation in the vacuole after a 4 h RALF1 treatment. VAMP711-RFP was the vacuole marker protein. RALF1, 1 µM; CHX, 50 µM. ***P*<0.01 (paired two-tailed Student's *t*-test). Data are mean±s.d. Scale bars: 10 µm.

for 1 h (Fig. 5C). We then performed the RALF1 treatment in the presence of the protein biosynthesis inhibitor CHX to determine whether the accumulation of FER-GFP at the TGN/endosome following RALF1 treatment was due to FER internalization from the PM or to *de novo* FER biosynthesis. Although CHX reduced the RALF1-induced accumulation of FER-GFP, significant quantities of FER-GFP were still detectable inside the cells (Fig. 5D). These data indicated that the accumulation of FER-GFP at the TGN after RALF1 treatment resulted from both the internalization and secretion of FER-GFP.

In keeping with the RALF1-enhanced internalization of FER, the fluorescence intensity of FER-GFP at the PM decreased after RALF1 treatment for 3 h (Fig. 5E). Fluorescence correlation spectroscopy (FCS), a robust technique for measuring changes in the fluorescence intensity of areas illuminated with a laser, showed that RALF1 treatment significantly reduced the mean density of FER-GFP at the PM, from 8.8 to 6.7 molecules/µm^2 (Fig. S4A). Furthermore, western blotting showed that the quantity of FER-GFP at the PM fell after RALF1 treatment for 3 h (Fig. S4B). These results strongly indicated that RALF1 enhanced FER-GFP internalization.

Additional experiments using the TGN marker protein VHA-a1-mRFP, the Golgi marker protein MEMB12-mCherry and the late endosome marker protein ARA7-RFP revealed that treatment with RALF1 for 3 h increased the colocalization of FER with the late endosome marker ARA7-RFP (Fig. 5F). We also observed FER-GFP accumulation in the vacuole after RALF1 treatment for 4 h (Fig. 5G). Some FER-GFP may thus be transported to the vacuole after RALF1-induced internalization.

The findings discussed above indicated that FER undergoes internalization by both CME and CIE. We therefore sought to determine which of these pathways mediated FER-GFP internalization following RALF1 treatment. Pretreatment with MβCD, which impairs CIE, had no effect on RALF1-induced endocytosis and the accumulation of FER-GFP in the vacuole (Fig. 6A), indicating that RALF1-induced internalization of FER-GFP to the vacuole was independent of CIE. To probe the role of CME, we performed experiments using an inducible line harboring a truncated plant CLATHRIN HEAVY CHAIN 1 (HUB-RFP), the overexpression of which blocks CME (Kitakura et al., 2011). After treating the transgenic plants with 4-hydroxytamoxifen for 48 h to induce HUB-RFP overexpression, HUB-RFP signals were detected and the internalization of FM4-64 was significantly inhibited, indicating that the overexpressed HUB-RFP was functional (Fig. S5). Moreover, after RALF1 treatment, the ratio of FER-GFP signal strength in the cytosol and the PM for the HUB-overexpressing line was significantly lower than in control seedlings (Fig. 6B). Dual-color fluorescence cross-correlation spectroscopy (FCCS) experiments in seedlings co-expressing *FER-GFP* with *CLC-mCherry* and *Flot1-mCherry* revealed that RALF1 treatment increased the relative cross-correlation amplitude of FER-GFP and CLC-mCherry from 0.526±0.09 to 0.743±0.12, but caused no significant change in the relative cross-correlation amplitude of FER-GFP and Flot1-mCherry (Fig. 6C-H). Together, these results

Development (2020) 147, dev189902. doi:10.1242/dev.189902

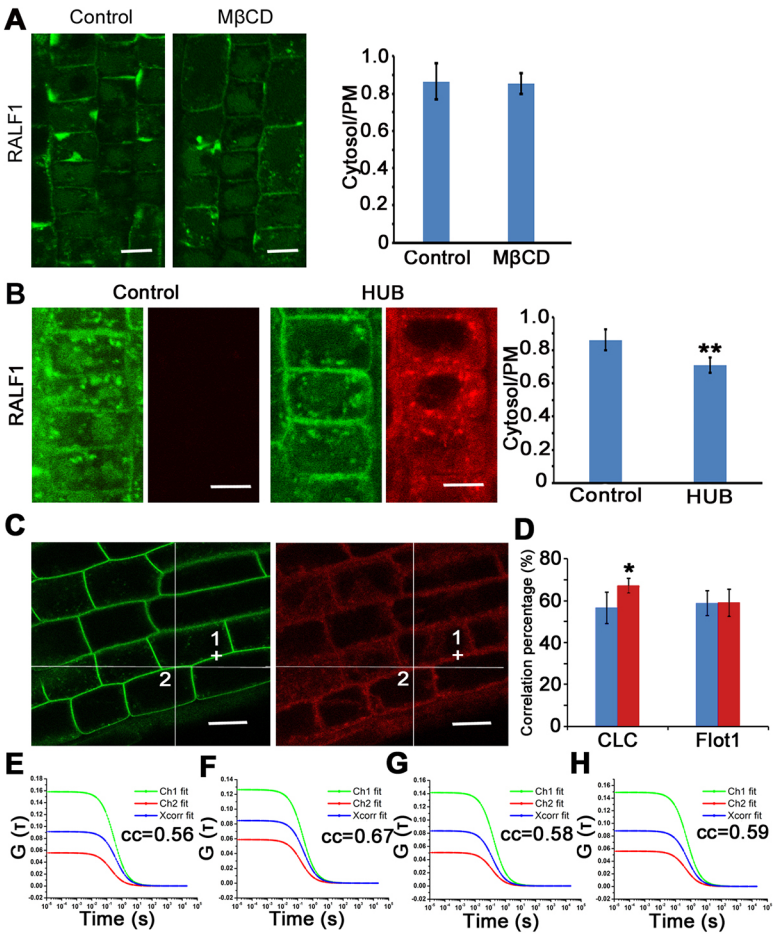

Fig. 6. CME was required for the internalization of FER-GFP after RALF1 treatment. (A) Left: RALF1-induced FER-GFP internalization after treatment with MβCD. *n*=42 for control and MβCD treatments. Scale bars: 20 µm. Right: quantification of FER-GFP signal strength in the cytosol and PM. (B) Left: RALF1-induced FER-GFP internalization in control and HUB-overexpressing root cells. Right: quantification of FER-GFP signal strength in the cytosol and PM of control and HUB-overexpressing root cells. *n*=27 for both lines. Scale bars: 10 µm. (C) Confocal images of FER-GFP and CLC-mCherry were analyzed using FCCS at points 1 and 2. *n*=88, 86, 126 and 82 points, respectively. Scale bars: 10 µm. (D) Correlations between FER-GFP and CLC-mCherry, and AtFlot1-mCherry with and without RALF1 treatment. (E,F) Fluorescence correlation curves of FER-GFP with CLC-mCherry without (E) and with (F) RALF1 treatment. (G,H) Fluorescence correlation curves of FER-GFP with Flot1-mCherry without (G) and with (H) RALF1 treatment. RALF1, 1 µM; MβCD, 10 mM. $^{**}P<0.01$, $^{*}P<0.05$ (paired two-tailed Student's *t*-test). Data are mean±s.d.

showed that CME was required for RALF1-induced FER-GFP internalization.

The RALF1-FER interaction also enhanced PIN2 and BRI1 internalization into the vacuole

The results presented above showed that RALF1 treatment enhanced the internalization of FER and its subsequent transport to the vacuole (Fig. 5G). We therefore investigated the effects of RALF1 on the internalization of three other PM proteins: PIN2-GFP, BRI1-GFP and LTi6a-GFP. Upon treatment with RALF1, the intensity of PIN2-GFP fluorescence at the PM decreased significantly and PIN2-GFP accumulated in the vacuole (Fig. 7A,B). However, PIN2-GFP localization was not affected by RALF1 in the *fer-4* mutant (Fig. 7C,D). Similar results were observed with BRI1-GFP (Fig. 7E-H). However, RALF1 treatment did not significantly reduce LTi6a-GFP fluorescence relative to that in control seedlings (Fig. S6). RALF1 thus affected the vacuolar internalization of FER and certain other PM proteins.

RALF1-induced inhibition of root growth involves CME

Ligand-RLK interactions are important for the downstream effects of these proteins, and the endocytic internalization of receptors has been found to be an essential component of their signaling pathways in many cases (Claus et al., 2018). The importance of CME in the internalization of FER-GFP was demonstrated by the results discussed above. Moreover, CME is also essential for the endocytosis of PIN2 and BRI1 (Dhonukshe et al., 2007; Kitakura et al., 2011; Irani et al., 2012; Di Rubbo et al., 2013). We therefore investigated its role in the RALF1-FER signaling pathway using the *clc2-1/3-1* mutant, which is impaired in CME (Wang et al., 2013a). In this mutant, RALF1 treatment increased the proportion of the FER-GFP population undergoing short-range diffusion from 23.7 to 35.0% (Fig. 8A-C) and reduced the diffusion coefficient of FER-GFP from $1.7403\pm0.3236\times10^{-2}$ to $1.0541\pm0.2354\times10^{-2}$ µm/s^2 (Fig. 8D-F). This restriction of FER-GFP dynamics following RALF1 treatment is similar to that observed in wild-type seedlings (Fig. 1C-H).

We next examined the activation of mitogen-activated protein kinases (MAPKs), a known RALF1 response (Pearce et al., 2001). The level of MAPK activation in the *clc2-1/3-1* mutant after RALF1 treatment was identical to that in the wild type (Fig. S7). Similarly, RALF1-induced changes in the gene expression of the *clc2-1/3-1* mutants were identical to those in the wild type (Fig. 8G,H).

We therefore analyzed the well-characterized inhibitory effect of RALF1 on root growth (Haruta et al., 2014). RALF1 inhibited root growth in both wild-type and *clc2-1/3-1* mutant seedlings. However, the degree of inhibition in the mutant seedlings was significantly lower than in the wild type (Fig. 8I,J). To exclude the possibility that this outcome was due to some specific property or function of CLC2, we also examined root growth in other CME-defective mutants, including *chc2-1*, *chc1-1* and *ap2m* (Bashline et al., 2013; Larson et al., 2017). These analyses also revealed that RALF1-induced inhibition of primary root growth was significantly attenuated in these CME mutants relative to the wild type (Fig. S8). Thus, the inhibition of root growth by RALF1 is also mediated via its effects on endocytosis.

Development (2020) 147, dev189902. doi:10.1242/dev.189902

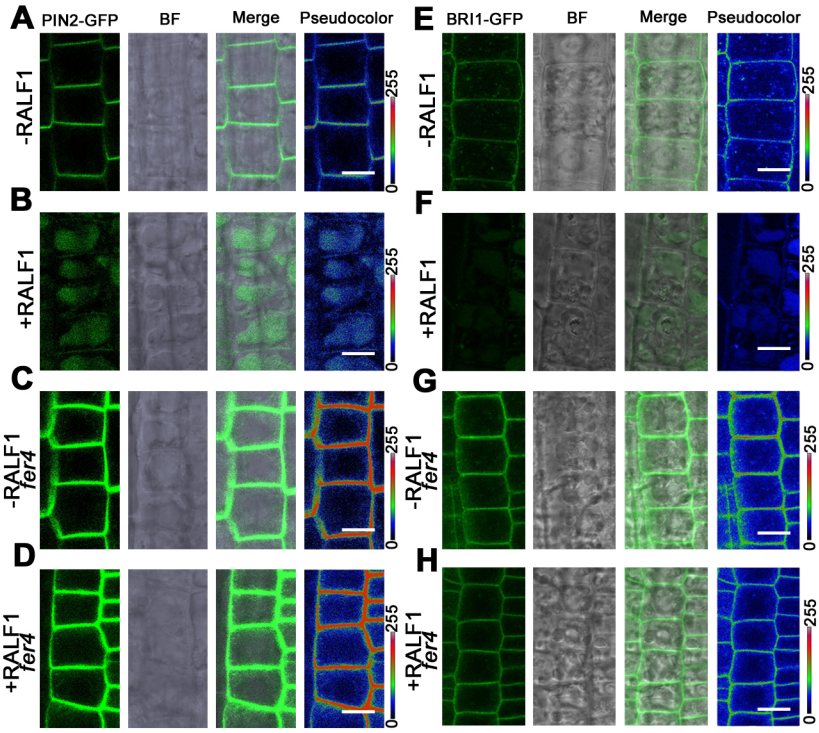

Fig. 7. RALF1 treatment enhanced the internalization of PIN2-GFP and BRI1-GFP to the vacuole. (A,B) PIN2-GFP fluorescence at the PM with and without RALF1 treatment for 3 h. (C,D) PIN2-GFP fluorescence at the PM with (D) and without (C) RALF1 treatment for 3 h. (E,F) BRI1-GFP fluorescence at the PM with (F) and without (E) RALF1 treatment for 3 h. (G,H) BRI1-GFP fluorescence at the PM in the *fer-4* mutant with (H) and without (G) RALF1 treatment for 3 h. RALF1, 1 µM. BF stands for bright field. Scale bars: 10 µm.

DISCUSSION

The RALF1-FER interaction plays a key role in various developmental responses in plants (Nissen et al., 2016). Membrane dynamics play an important role in the functionality of RLKs. However, much less is known about the PM dynamics and trafficking of FER, the extent to which RALF1-dependent signaling affects these processes, and whether the interaction between RALF1 and the dynamics of FER modulate signaling via FER.

RLKs localized to the PM display dynamic behavior (Li et al., 2013). In this work, we used VA-TIRFM to quantitatively monitor the spatial and temporal dynamics of FER-GFP molecules, revealing that this protein displays dynamic behavior at the PM. Moreover, the lateral diffusion of FER-GFP at the PM was complex; four distinct types of diffusion were identified: Brownian, restricted, directed and mixed diffusion. A complementary single-particle tracking analysis revealed that FER is heterogeneously distributed on the PM.

Several studies have recently shown that the mobility of PM proteins is controlled by their ligands, which play important roles in their function (Wang et al., 2015; Cui et al., 2018; Xue et al., 2018). For example, the diffusion coefficient and motion range of FLS2 both increase in response to its ligand, flg22 (Cui et al., 2018). Conversely, the mobility of the mammalian PM receptor EGFR is reduced by treatment with EGF (Low-Nam et al., 2011), which might facilitate the formation of stable receptor oligomers to deliver signals. Xiao et al. (2019) showed that RALF23 treatment induces the heterodimerization of LLG proteins with the ectodomain of FER, and LLG1 is a GPI anchor protein that is mostly located in membrane rafts, indicating that RALF23 treatment might facilitate FER enrichment in membrane rafts (Borner et al., 2005; Xiao et al., 2019). Consistent with this work, RALF1 treatment increased the amount of FER-GFP in membrane rafts relative to that outside rafts (Fig. 1I,J). Moreover, Du et al. (2016) revealed that RALF1-FER signal transduction depends on the formation of a FER-RIPK complex (Du et al., 2016). Here, we found that the motion range and diffusion coefficient of FER-GFP at the PM were both reduced by RALF1 treatment (Fig. 1C-H). Although the functional significance of this RALF1-mediated reduction in the diffusion coefficient of FER remains unclear, the RALF1-induced confinement of FER in microdomains, and reduction of its mobility, might facilitate FER-RIPK complex formation.

Changes in the homo-oligomeric state of PM proteins, induced by specific ligands or other triggers, play crucial roles in certain signal transduction processes (Schlessinger, 2002). For example, Xue et al. (2018) recently found that the blue-light-induced homodimerization of PHOT1 is important for PHOT1-mediated signaling (Xue et al., 2018). Although RALF1 treatment contributes to nucleate the assembly of RALF23-LLG1-FER and FER-RIPK heterocomplexes, the homo-oligomerization of FER is still unknown (Du et al., 2016; Xiao et al., 2019). We therefore investigated whether RALF1 modulates FER homo-oligomerization and found that FER mainly exists as a monomer at the PM (Fig. 2), with no evidence that RALF1 induced FER multimerization. In this respect, FER resembles BRI1, which undergoes homodimerization independently of its brassinosteroid ligand (Hink et al., 2008).

Endocytosis-mediated internalization plays a crucial role in maintaining RLK homeostasis at the PM and the associated signal transduction activity (Claus et al., 2018). In plant cells, PM proteins can be endocytosed via CME or CIE; some proteins such as RbohD and PIP2;1 are transported by both pathways under normal growth conditions (Li et al., 2011; Hao et al., 2014). Our data showed that CME and CIE cooperatively regulate the internalization of FER under steady-state conditions (Fig. 4). Moreover, RLKs can be endocytosed either independently of binding to their ligand or in response to it (Beck et al., 2012). A previous study showed that RALF23 treatment also induced the internalization of FER-GFP (Zhao et al., 2018). We found that the density of FER-GFP at the PM decreased after RALF1 treatment (Fig. 5E, Fig. S4). All of these results imply that there is more than one RALF that can interact with FER to enhance the internalization of FER. The balance between

Development (2020) 147, dev189902. doi:10.1242/dev.189902

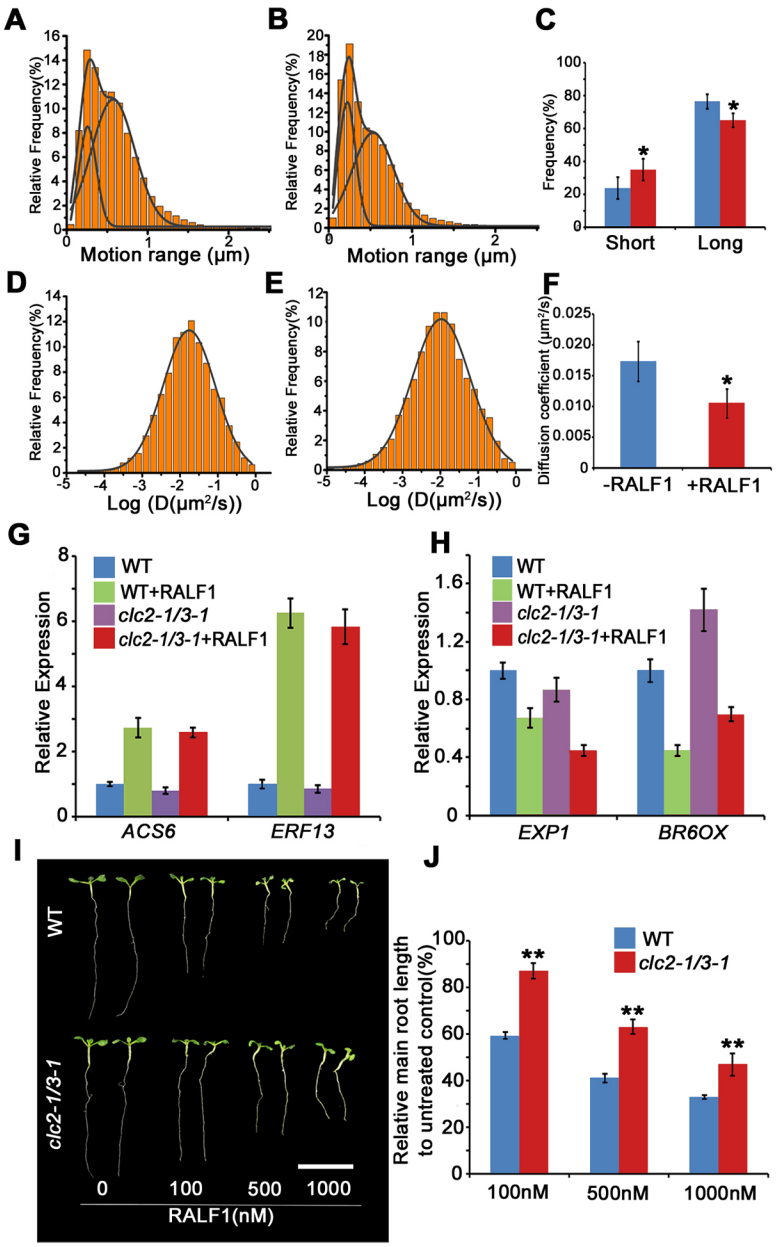

Fig. 8. RALF1-induced inhibition of root growth rather than early signaling transduction is affected in *clc2-1/3-1* mutant. (A) Distribution of FER-GFP movement distances in the root cells in the *clc2-1/3-1* mutant (n=16,841 spots). (B) Distribution of FER-GFP movement distances in the *clc2-1/3-1* mutant after treatment with 1 μM RALF1 (n=18,637 spots). (C) Comparison of FER-GFP movement distances in the *clc2-1/3-1* mutant with and without RALF1 treatment. (D) Distribution of FER-GFP diffusion coefficients in the root cells in the *clc2-1/3-1* mutant (n=3494 spots). (E) Distribution of FER-GFP diffusion coefficients in the *clc2-1/3-1* mutant after treatment with 1 μM RALF1 (n=3648 spots). (F) Comparison of FER-GFP diffusion coefficients in the *clc2-1/3-1* mutant with and without RALF1 treatment. (G,H) Expression of the RALF1-regulated genes *ACS6*, *ERF6*, *EXP1* and *BR6OX* in the wild type (WT) and the *clc2-1/3-1* mutant. (I,J) RALF1-induced root growth inhibition in the *clc2-1/3-1* mutant. n=15 roots for every experiment. RALF1, 1 μM. $^{**}P$<0.01, $^{*}P$<0.05, t-test. Data are mean±s.d. Scale bar: 1 cm.

internalization via CME and CIE is regulated by specific signals or stimuli (Mayor and Pagano, 2007); for example, NaCl treatment enhanced the endocytosis of PIP2;1 and RbohD by CIE (Li et al., 2011; Hao et al., 2014). Our results indicate that FER is internalized via both the CME and CIE pathways, and that RALF1 alters the balance of FER internalization between these pathways by enhancing the contribution of CME.

Ligands can affect the trafficking of their receptors. For example, under steady-state conditions, FLS2 is mainly localized at the PM and partially recycled between the TGN and the PM. However, treatment with flg22 causes it to be sorted to the vacuole following endocytosis (Mbengue et al., 2016). Here, we found that RALF1 treatment caused FER to accumulate in the TGN and then be transported to the vacuole (Fig. 5G), i.e. RALF1 altered the trafficking of FER.

RALF1 also affected the internalization and trafficking of other proteins. Many studies have investigated how ligands can affect endocytosis and trafficking of their receptors but few have examined the potential for ligand-receptor pairs to affect the internalization and trafficking of other PM proteins. Jing et al. (2019) found that the PLANT ELICITOR PEPTIDE 1 (PEP1)/PLANT ELICITOR PEPTIDE RECEPTOR 2 (PEPR2) pair can regulate PIN2 levels at the PM by controlling its endocytosis (Jing et al., 2019). In keeping with this result, we found that the RALF1-FER interaction also regulates the levels of the PM proteins PIN2 and BRI1 at the PM by controlling their internalization, indicating that FER is an important regulator of PM protein endocytosis (Fig. 7). Previous studies showed that RALF1-overexpressing plants exhibited no increase in root length and no change in the number of emerging lateral roots after brassinolide treatment, indicating that RALF1 overexpression reduced sensitivity to exogenous brassinolide in *Arabidopsis* seedlings (Bergonci et al., 2014). Our results showed that BRI1-GFP fluorescence decreased significantly after RALF1 treatment, indicating that RALF1 reduced the levels of PM-localized BRI1 and therefore reduced the ability of the cells to detect exogenous brassinolide. This might be the mechanism responsible for the

Development (2020) 147, dev189902. doi:10.1242/dev.189902

reduction in exogenous brassinolide sensitivity in seedlings overexpressing RALF1.

RLKs are known to induce signaling pathway activity at the PM upon the binding of their ligands (Haruta et al., 2017). For example, RALF1-FER signal transduction depends on the formation of a FER-RIPK complex at the PM (Du et al., 2016). Here, we showed that RALF1 treatment limited the dynamics of FER-GFP and enhanced the ratio of FER-GFP in membrane rafts, indicating that signaling transduction at the PM induced by RALF1-FER interaction is complex and important. In addition, the subcellular trafficking of PM receptors also plays a vital role in signal transduction (Claus et al., 2018). For example, Spallek et al. (2013) found that the endosome trafficking of FLS2 is crucial for flg22-activated stomatal defenses (Spallek et al., 2013). Moreover, CME is an organizer of this cellular signaling and was shown to contribute to the regulation of callose deposition and stomatal closure (but not MAPK activation) following flg22 treatment (Mbengue et al., 2016). However, PEP1-PEPR1 interaction-mediated MAPK activation was strongly reduced when CME was blocked, implying that CME is closely associated with PEP1-induced signaling (Ortiz-Morea et al., 2016). In keeping with this result, we found that CME plays a crucial role in RALF1-induced inhibition of root growth but does not affect early signaling transduction (Fig. 8). By using VA-TIRFM to monitor the movement of FER-GFP at the PM following RALF1 treatment, we found that the dynamic changes in the FER distribution in *fer-4* and *clc2-1/3-1* mutants were similar to those in wild-type seedlings. This indicates that FER retained its functionality at the PM, which might explain why early signal transduction in the *clc2-1/3-1* mutant was unaffected by RALF1 treatment (Fig. 8A-F). CME is important for the internalization and trafficking to the vacuole of several PM proteins (Chen et al., 2011). We found that RALF1 treatment enhanced the internalization of several PM proteins and caused their accumulation in the vacuole, which suggests that CME-defective mutants are less sensitive to RALF1 because RALF1 acts (at least in part) by inducing the CME-mediated internalization of PM proteins.

In summary, previous studies on RALF1-FER signaling focused primarily on signaling events that occur at the PM. As a result, little was known about the trafficking of FER and the impact of its interaction with RALF1 on its function and trafficking. Thus, the results presented here further extend our understanding into the mode of signaling of RALF1 and FER, and suggest that they can also mediate the regulation of plant growth via their effects on the endocytosis and trafficking of PM proteins (Fig. S9).

MATERIALS AND METHODS

Plant materials and growth conditions

The *Arabidopsis thaliana* lines used in this study were Col-0, FER-GFP/*fer4*, Flot1-mCherry, CLC-mCherry, VHA-a1-RFP, MEMB12-mCherry, ARA7-RFP, HUB-RFP, PIN2-GFP, BRI1-GFP, *fer-4*, *clc2-1/3-1*, *chc2-1*, *chc1-1* and *ap2m* (Geldner et al., 2007; Duan et al., 2010; Park et al., 2016; Yu et al., 2017). Dual-marker lines were generated by crossing FER-GFP with plants expressing different organelle marker proteins.

Arabidopsis seeds were surface sterilized for 30 s in 85% ethanol/H_2O_2 and stratified at 4°C for 2 days in darkness. The seedlings were then grown on vertical plates containing half-strength Murashige and Skoog (MS) medium in a growth chamber with a constant temperature of 22°C and 16 h light/8 h dark cycles.

Drug treatments

The RALF1 peptides were synthesized by SciLight Biotechnology and used at a concentration of 1 µM in half-strength MS growth medium. Other chemicals used in this work were purchased from Sigma-Aldrich unless otherwise indicated, and were used at the following working concentrations: FM4-64, 5 µM; BFA, 50 µM; CHX, 50 µM; Conc A, 2 µM; 4-hydroxytamoxifen, 2 µM; and MβCD, 10 mM. All of these chemicals were diluted using half-strength MS growth medium, and the chemical treatments were performed as reported previously (Wang et al., 2015).

Confocal microscopy and image analysis

Confocal microscopy was performed using a Leica TCS SP8 confocal microscope fitted with a 63× oil-immersion objective. GFP/FM4-64 and RFP/mCherry were excited at wavelengths of 488 nm and 561 nm, respectively. Emitted fluorescence was detected at 500 nm to 545 nm for GFP, 600 nm to 700 nm for FM4-64, and 580 nm to 620 nm for RFP/mCherry. All images were acquired using the same parameter settings and quantified using ImageJ software (National Institutes of Health). At least three cells per root for five seedlings were measured to analyze the colocalization of FER-GFP with other endosome marker proteins. To quantify relative signal intensity, the mean pixel intensity of the cytosol and the PM were measured using ImageJ. Finally, the ratios of the intensity values were calculated.

VA-TIRFM live imaging and single-particle fluorescence image analysis

Seedlings were treated with half-strength MS media containing RALF1 or with RALF1-free control media for 15 min, then observed using the VA-TIRFM microscope. VA-TIRFM was performed as described previously (Cui et al., 2018), using an inverted IX71 microscope (Olympus) with a totally internally reflective fluorescence illuminator and a 100× oil-immersion objective (Olympus; numerical aperture, 1.45). To track the mobility of FER-GFP particles at the PM, the epidermal cells of 4-day-old *Arabidopsis* roots were observed using VA-TIRFM and repeatedly imaged with an exposure time of 100 ms to create movies. Each movie included 100 time-lapse images. FER-GFP was excited with 473 nm light from a diode laser (Changchun New Industries Optoelectronics Tech), and the emitted GFP fluorescence was filtered using a BA510IF filter (Olympus). The FER-GFP fluorescent signals were recorded using a digital Andor iXon DV8897D-CS0-VP EMCCD camera after filtering with two band-pass filters (525/545 nm). The single-particle tracking analysis procedure was described previously (Wang et al., 2015). At least three cells per seedling from three seedlings were analyzed.

The stepwise photobleaching of FER-GFP at the PM was analyzed using 'progressive idealization and filtering' (PIF) software. First, we obtained the series of images of FER-GFP at the PM by TIRFM. Then, the rolling ball method in ImageJ software was used to subtract the background of these images. Finally, we used the automated analysis program PIF to analyze the stepwise photobleaching (McGuire et al., 2012).

BiFC analysis

For the BiFC analysis, the *YFP* gene was cut into two sections (*nYFP* and *cYFP*), which were separately cloned into the pCAMBIA2300-35S-GFP vector to replace GFP. The resulting vectors were named 35S::nYFP and 35S::cYFP. *FER* (primers: 5′-GCAGAATTCCTCCGAAGCTTTCAAG-TGTGATTG-3′ and 5′-GCAGGATCCACGTCCCTTTGGATTCATGAT-C-3′) and *SAM1* (primers: 5′-CGGGGTACCATGGAGACTTTTCT-ATTCACAT-3′ and 5′-CGCGGATCCGCTTGAGGTTTGTCCCACTTG-A-3′) were cloned by PCR, and subcloned into the *35S::nYFP* and *35S::cYFP* vectors, respectively. The resulting constructs were transferred into *Agrobacterium tumefaciens* GV3101 and infiltrated into the abaxial sides of *Nicotiana tabacum* (L.) leaves (OD_{600}=0.5), individually or in combination. The plants were then grown in darkness for 36 h, after which their fluorescence was imaged using a Leica TCS SP8 confocal laser scanning microscope with a 514 nm laser.

Immunoblotting

Seedlings (10 days old) were treated with RALF1 or a control solution for the indicated time and then ground to fine powder in liquid nitrogen. Total proteins were then extracted using buffer E [100 ml of buffer E contains 1.5125 g Tris-HCl (pH 8.8), 11.1 ml glycerin, 1.2409 g $Na_2S_2O_5$, 5 mM DTT and 1 g SDS]. For the sucrose gradient ultracentrifugation experiment,

we added the buffer with total proteins to the tube overlaid with successive 3 ml steps of 40, 35, 30, 10 and 5% sucrose in buffer E, which was then centrifuged for 18 h at 230,000 ***g*** in a TST41 rotor (Sorvall). After this, the buffer was divided into 11 equal parts for western blotting. For PM protein extraction, the powder was ground in ice-cold buffer [20 mM Tris-HCl (pH 8.8), 150 mM NaCl, 1 mM EDTA, 20% glycerol, 1 mM phenylmethylsulfonyl (PMSF), 10 µg/ml chymostatin, 1 µg/ml leupeptine and 10 µg/ml aprotinin]. The sample was then centrifuged at 6000 ***g*** for 15 min at 4°C, and the resulting supernatant was further centrifuged at 100,000 ***g*** for 25 min at 4°C to pellet the total membrane fraction. The pellet was redissolved using a buffer containing 10 mM Tris-HCl (pH 7.3), 150 mM NaCl, 1 mM PMSF, 1 mM EDTA, 1% Triton X-100, 10% glycerol, 1 g/ml leupeptine, 10 g/ml chymostatin and 10 g/ml aprotinin to release the membrane proteins. The resulting solution was centrifuged at 100,000 ***g*** for another 25 min at 4°C to separate the insoluble and solubilized membrane proteins. The proteins were separated on a 10% SDS-polyacrylamide gel, after which they were transferred to a nitrocellulose membrane. Protein detection was performed using the following antibodies: anti-FER antibody (1:4000; Du et al., 2016), anti-GFP antibody (1:1000, AT0028, CMC), anti-AHA antibody (1:2000, AS07 260, Agrisera), and anti-MAPK antibody (1:1000, AM063, Beyotime Biotechnology).

FCS and fluorescence cross-correlation spectroscopy (FCCS) analysis

FCS analysis was conducted in point scanning mode using a Leica TCS SP5 FCS microscope equipped with a 488 nm argon laser, a coupled correlator built in-house and an avalanche photodiode. The laser was focused on selected areas of the PM. Under these conditions, changes in the local concentration of fluorophores resulted in spontaneous fluctuations in fluorescence intensity that could be detected and used to calculate the FER-GFP density as previously described (Li et al., 2011).

To analyze the correlations between FER-GFP with CLC-mCherry or Flot1-mCherry, FCCS was performed using a Leica TCS SP5 microscope as described previously (Li et al., 2011). GFP and mCherry-labeled proteins were excited with 488 nm and 561 nm lasers, respectively. BP 505-540 and LP 580 emission filters were used for the green and red channels, respectively. When the two spectrally distinct molecules moved together through the focal volume, their motion was correlated and the resulting signal contributed to the cross-correlation curve. The relative cross-correlation was then calculated as described previously (Li et al., 2011). Analyses were performed at 30 locations on the PM in five different seedlings.

Quantitative real-time PCR (qRT-PCR)

Total RNA was extracted from 10-day-old *Arabidopsis* seedlings using a Tiangen NApre Plant Kit (Tiangen) in accordance with the manufacturer's instructions. Reverse transcription was performed using a FastQuant RT Kit (Tiangen) and qRT-PCR was performed using TB Green (Takara). The RALF1-responsive marker genes and the primers used for qRT-PCR were as follows: *ACS6* (At4g11280, 5′-AGGGATTGGTTGGTTAAAGG-3′ and 5′-TGAGCTTCACTTGGTGAACA-3′), *ERF13* (At2g44840, 5′-TGAATTTTCCGCATTTGATT-3′ and 5′-CAAACTAGACTCGCCGTCAT-3′), *EXP1* (At1g69530, 5′-GCGTGAGAAGAGGAGGAATA-3′ and 5′-AACCTTTAACCATCGCTGAG-3′) and *BR6OX2* (At3g30180, 5′-TCTTTGGAGGTGGAGTTAGG-3′ and 5′-TTCTTCCATTCTCTTCCCATC-3′) (Haruta et al., 2014). qRT-PCR was performed in triplicate for each of the three biological replicates. Data were collected and analyzed using an Eppendorf real-time PCR detection system (Eppendorf).

Measurement of root length

Seeds were germinated on vertically positioned half-strength MS media plates for 3 days, transferred to half-strength MS liquid media containing the RALF1 peptides or a control solution, and left to grow for another 3 days. The seedlings were then photographed and eight roots were analyzed using ImageJ. Three biological replicates were performed.

Accession numbers

Sequence data associated with this article can be found in the Arabidopsis Genome Initiative or GenBank/EMBL databases under the following accession numbers: *FER* (At3g51550), *FLOT1* (At5g25250), *CLC2* (At2g40060), *SAM1* (At1g02500), *VHA-A1* (At2g28520), *MEMB12* (AT5G50440), *ARA7* (AT4G19640), *VAMP711* (AT4G32150), *BRI1* (AT4G39400) and *PIN2* (AT5G57090).

Acknowledgements

We thank Prof. Inhwan Hwang for providing us with the INTAM≫HUB-RFP seedlings and Prof. Ruixi Li for providing us with the seed expression, Golgi, late endosome and vacuole marker proteins.

Competing interests

The authors declare no competing or financial interests.

Author contributions

Conceptualization: M.Y., R.L., Y. Cui, R.B., F.Y., J.L.; Methodology: M.Y., R.L., Y. Cui, X.Z., Y.B., Y. Cao, J.X.; Software: M.Y., R.L., Y. Cui, W.C., B.L., X.Z., Y.B., Y. Cao; Validation: R.L., W.C., B.L.; Formal analysis: M.Y., W.C., J.X.; Investigation: B.L., X.Z., J.X.; Data curation: Y. Cao; Writing - original draft: M.Y., P.K.J., X.L., R.B., F.Y., J.L.; Writing - review & editing: F.Y., J.L.; Visualization: P.K.J.; Supervision: R.B.; Project administration: R.B., F.Y., J.L.; Funding acquisition: J.L.

Funding

This work was supported by the National Natural Science Foundation of China (31530084 to J.L., 31761133009 to J.L., 31670182 to R.L., 91954202 to X.L., 31401149 to R.L. and 31970182 to R.L.); the Beijing Forestry University Outstanding Young Talent Cultivation Project (2019JQ03003 to X.L.); the Fundamental Research Funds for the Central Universities (2019ZY29 and 2017ZY10 to R.L.); the Program of Introducing Talents of Discipline to Universities (111 project, B13007 to J.L.); and the China Postdoctoral Science Foundation (2019M660497 to M.Y.).

Supplementary information

Supplementary information available online at
https://dev.biologists.org/lookup/doi/10.1242/dev.189902.supplemental

Peer review history

The peer review history is available online at
https://dev.biologists.org/lookup/doi/10.1242/dev.189902.reviewer-comments.pdf

References

Bashline, L., Li, S., Anderson, T., Lei, L. and Gu, Y. (2013). The endocytosis of cellulose synthase in *Arabidopsis* is dependent on µ2, a clathrin-mediated endocytosis adaptin. *Plant Physiol.* **163**, 150-160. doi:10.1104/pp.113.221234

Beck, M., Zhou, J., Faulkner, C., MacLean, D. and Robatzek, S. (2012). Spatio-temporal cellular dynamics of the *Arabidopsis* flagellin receptor reveal activation status-dependent endosomal sorting. *Plant Cell* **24**, 4205-4219. doi:10.1105/tpc.112.100263

Bergonci, T., Ribeiro, B., Ceciliato, P. H. O., Guerrero-Abad, J. C., Silva-Filho, M. C. and Moura, D. S. (2014). *Arabidopsis thaliana* RALF1 opposes brassinosteroid effects on root cell elongation and lateral root formation. *J. Exp. Bot.* **65**, 2219-2230. doi:10.1093/jxb/eru099

Boisson-Dernier, A., Kessler, S. A. and Grossniklaus, U. (2011). The walls have ears: the role of plant CrRLK1Ls in sensing and transducing extracellular signals. *J. Exp. Bot.* **62**, 1581-1591. doi:10.1093/jxb/erq445

Borner, G. H. H., Sherrier, D. J., Weimar, T., Michaelson, L. V., Hawkins, N. D., MacAskill, A., Napier, J. A., Beale, M. H., Lilley, K. S. and Dupree, P. (2005). Analysis of detergent-resistant membranes in *Arabidopsis*. Evidence for plasma membrane lipid rafts. *Plant Physiol.* **137**, 104-116. doi:10.1104/pp.104.053041

Chen, X., Irani, N. G. and Friml, J. (2011). Clathrin-mediated endocytosis: the gateway into plant cells. *Curr. Opin. Plant Biol.* **14**, 674-682. doi:10.1016/j.pbi.2011.08.006

Claus, L. A. N., Savatin, D. V. and Russinova, E. (2018). The crossroads of receptor-mediated signaling and endocytosis in plants. *J. Integr. Plant Biol.* **60**, 827-840. doi:10.1111/jipb.12672

Cui, Y., Li, X., Yu, M., Li, R., Fan, L., Zhu, Y. and Lin, J. (2018). Sterols regulate endocytic pathways during flg22-induced defense responses in *Arabidopsis*. *Development* **145**, dev.165688. doi:10.1242/dev.165688

Cui, Y., Zhang, X., Yu, M., Zhu, Y., Xing, J. and Lin, J. (2019). Techniques for detecting protein-protein interactions in living cells: principles, limitations, and recent progress. *Sci. China Life Sci.* **62**, 619-632. doi:10.1007/s11427-018-9500-7

Dhonukshe, P., Aniento, F., Hwang, I., Robinson, D. G., Mravec, J., Stierhof, Y.-D. and Friml, J. (2007). Clathrin-mediated constitutive endocytosis of PIN auxin efflux carriers in *Arabidopsis*. *Curr. Biol.* **17**, 520-527. doi:10.1016/j.cub.2007.01.052

Di Rubbo, S., Irani, N. G., Kim, S. Y., Xu, Z.-Y., Gadeyne, A., Dejonghe, W., Vanhoutte, I., Persiau, G., Eeckhout, D., Simon, S. et al. (2013). The clathrin adaptor complex AP-2 mediates endocytosis of brassinosteroid insensitive1 in *Arabidopsis*. *Plant Cell* **25**, 2986-2997. doi:10.1105/tpc.113.114058

Douglass, A. D. and Vale, R. D. (2005). Single-molecule microscopy reveals plasma membrane microdomains created by protein-protein networks that exclude or trap signaling molecules in T cells. *Cell* **121**, 937-950. doi:10.1016/j.cell.2005.04.009

Dressano, K., Ceciliato, P. H. O., Silva, A. L., Guerrero-Abad, J. C., Bergonci, T., Ortiz-Morea, F. A., Burger, M., Silva-Filho, M. C. and Moura, D. S. (2017). BAK1 is involved in AtRALF1-induced inhibition of root cell expansion. *PLoS Genet.* **13**, e1007053. doi:10.1371/journal.pgen.1007053

Du, C., Li, X., Chen, J., Chen, W., Li, B., Li, C., Wang, L., Li, J., Zhao, X., Lin, J. et al. (2016). Receptor kinase complex transmits RALF peptide signal to inhibit root growth in *Arabidopsis*. *Proc. Natl. Acad. Sci. USA* **113**, E8326-E8334. doi:10.1073/pnas.1609626113

Duan, Q., Kita, D., Li, C., Cheung, A. Y. and Wu, H.-M. (2010). FERONIA receptor-like kinase regulates RHO GTPase signaling of root hair development. *Proc. Natl. Acad. Sci. USA* **107**, 17821-17826. doi:10.1073/pnas.1005366107

Fan, L., Li, R., Pan, J., Ding, Z. and Lin, J. (2015). Endocytosis and its regulation in plants. *Trends Plant Sci.* **20**, 388-397. doi:10.1016/j.tplants.2015.03.014

Ge, Z., Bergonci, T., Zhao, Y., Zou, Y., Du, S., Liu, M.-C., Luo, X., Ruan, H., Garcia-Valencia, L. E., Zhong, S. et al. (2017). *Arabidopsis* pollen tube integrity and sperm release are regulated by RALF-mediated signaling. *Science* **358**, 1596-1600. doi:10.1126/science.aao3642

Geldner, N., Hyman, D. L., Wang, X., Schumacher, K. and Chory, J. (2007). Endosomal signaling of plant steroid receptor kinase BRI1. *Genes Dev.* **21**, 1598-1602. doi:10.1101/gad.1561307

Guo, H., Li, L., Ye, H., Yu, X., Algreen, A. and Yin, Y. (2009). Three related receptor-like kinases are required for optimal cell elongation in *Arabidopsis thaliana*. *Proc. Natl. Acad. Sci. USA* **106**, 7648-7653. doi:10.1073/pnas.0812346106

Hao, H., Fan, L., Chen, T., Li, R., Li, X., He, Q., Botella, M. A. and Lin, J. (2014). Clathrin and membrane microdomains cooperatively regulate RbohD dynamics and activity in *Arabidopsis*. *Plant Cell* **26**, 1729-1745. doi:10.1105/tpc.113.122358

Haruta, M. and Sussman, M. R. (2017). Ligand receptor-mediated regulation of growth in plants. *Curr. Top. Dev. Biol.* **123**, 331-363. doi:10.1016/bs.ctdb.2016.11.007

Haruta, M., Sabat, G., Stecker, K., Minkoff, B. B. and Sussman, M. R. (2014). A peptide hormone and its receptor protein kinase regulate plant cell expansion. *Science* **343**, 408-411. doi:10.1126/science.1244454

Hink, M. A., Shah, K., Russinova, E., de Vries, S. C. and Visser, A. J. W. G. (2008). Fluorescence fluctuation analysis of *Arabidopsis thaliana* somatic embryogenesis receptor-like kinase and brassinosteroid insensitive 1 receptor oligomerization. *Biophys. J.* **94**, 1052-1062. doi:10.1529/biophysj.107.112003

Huck, N., Moore, J. M., Federer, M. and Grossniklaus, U. (2003). The *Arabidopsis* mutant *feronia* disrupts the female gametophytic control of pollen tube reception. *Development* **130**, 2149-2159. doi:10.1242/dev.00458

Irani, N. G., Di Rubbo, S., Mylle, E., Van den Begin, J., Schneider-Pizoń, J., Hniliková, J., Šíša, M., Buyst, D., Vilarrasa-Blasi, J., Szatmári, A.-M. et al. (2012). Fluorescent castasterone reveals BRI1 signaling from the plasma membrane. *Nat. Chem. Biol.* **8**, 583-589. doi:10.1038/nchembio.958

Jing, Y., Zheng, X., Zhang, D., Shen, N., Wang, Y., Yang, L., Fu, A., Shi, J., Zhao, F., Lan, W. et al. (2019). Danger-Associated Peptides Interact with PIN-Dependent Local Auxin Distribution to Inhibit Root Growth in *Arabidopsis*. *Plant Cell* **31**, 1767-1787. doi:10.1105/tpc.18.00757

Kessler, S. A., Shimosato-Asano, H., Keinath, N. F., Wuest, S. E., Ingram, G., Panstruga, R. and Grossniklaus, U. (2010). Conserved molecular components for pollen tube reception and fungal invasion. *Science* **330**, 968-971. doi:10.1126/science.1195211

Kitakura, S., Vanneste, S., Robert, S., Löfke, C., Teichmann, T., Tanaka, H. and Friml, J. (2011). Clathrin mediates endocytosis and polar distribution of PIN auxin transporters in *Arabidopsis*. *Plant Cell* **23**, 1920-1931. doi:10.1105/tpc.111.083030

Larson, E. R., van Zelm, E., Roux, C., Marion-Poll, A. and Blatt, M. R. (2017). Clathrin heavy chain subunits coordinate endo- and exocytic traffic and affect stomatal movement. *Plant Physiol.* **175**, 708-720. . doi:10.1104/pp.17.00970

Li, X., Wang, X., Yang, Y., Li, R., He, Q., Fang, X., Luu, D.-T., Maurel, C. and Lin, J. (2011). Single-molecule analysis of PIP2;1 dynamics and partitioning reveals multiple modes of *Arabidopsis* plasma membrane aquaporin regulation. *Plant Cell* **23**, 3780-3797. doi:10.1105/tpc.111.091454

Li, R., Liu, P., Wan, Y., Chen, T., Wang, Q., Mettbach, U., Baluška, F., Šamaj, J., Fang, X., Lucas, W. J. et al. (2012). A membrane microdomain-associated protein, *Arabidopsis* Flot1, is involved in a clathrin-independent endocytic pathway and is required for seedling development. *Plant Cell* **24**, 2105-2122. doi:10.1105/tpc.112.095695

Li, X., Luu, D.-T., Maurel, C. and Lin, J. (2013). Probing plasma membrane dynamics at the single-molecule level. *Trends Plant Sci.* **18**, 617-624. doi:10.1016/j.tplants.2013.07.004

Liao, H., Tang, R., Zhang, X., Luan, S. and Yu, F. (2017). FERONIA Receptor Kinase at the Crossroads of Hormone Signaling and Stress Responses. *Plant Cell Physiol.* **58**, 1143-1150. doi:10.1093/pcp/pcx048

Lindner, H., Müller, L. M., Boisson-Dernier, A. and Grossniklaus, U. (2012). CrRLK1L receptor-like kinases: not just another brick in the wall. *Curr. Opin. Plant Biol.* **15**, 659-669. doi:10.1016/j.pbi.2012.07.003

Low-Nam, S. T., Lidke, K. A., Cutler, P. J., Roovers, R. C., van Bergen en Henegouwen, P. M. P., Wilson, B. S. and Lidke, D. S. (2011). ErbB1 dimerization is promoted by domain co-confinement and stabilized by ligand binding. *Nat. Struct. Mol. Biol.* **18**, 1244-1249. doi:10.1038/nsmb.2135

Luo, Y., Scholl, S., Doering, A., Zhang, Y., Irani, N. G., Rubbo, S. D., Neumetzler, L., Krishnamoorthy, P., Van Houtte, I., Mylle, E. et al. (2015). V-ATPase activity in the TGN/EE is required for exocytosis and recycling in *Arabidopsis*. *Nat. Plants* **1**, 15094. doi:10.1038/nplants.2015.94

Mao, D., Yu, F., Li, J., Van de Poel, B., Tan, D., Liu, Y., Li, X., Dong, M., Chen, L., Li, D. et al. (2015). FERONIA receptor kinase interacts with S-adenosylmethionine synthetase and suppresses S-adenosylmethionine production and ethylene biosynthesis in *Arabidopsis*. *Plant Cell Environ.* **38**, 2566-2574. doi:10.1111/pce.12570

Mayor, S. and Pagano, R. E. (2007). Pathways of clathrin-independent endocytosis. *Nat. Rev. Nat. Rev. Mol. Cell Biol.* **8**, 603-612. doi:10.1038/nrm2216

Mbengue, M., Bourdais, G., Gervasi, F., Beck, M., Zhou, J., Spallek, T., Bartels, S., Boller, T., Ueda, T., Kuhn, H. et al. (2016). Clathrin-dependent endocytosis is required for immunity mediated by pattern recognition receptor kinases. *Proc. Natl. Acad. Sci. USA* **113**, 11034-11039. doi:10.1073/pnas.1606004113

McGuire, H., Aurousseau, M. R. P., Bowie, D. and Blunck, R. (2012). Automating single subunit counting of membrane proteins in mammalian cells. *J. Biol. Chem.* **287**, 35912-35921. doi:10.1074/jbc.M112.402057

Nebenfuhr, A., Ritzenthaler, C. and Robinson, D. G. (2002). Brefeldin A: deciphering an enigmatic inhibitor of secretion. *Plant Physiol.* **130**, 1102-1108. doi:10.1104/pp.011569

Nissen, K. S., Willats, W. G. T. and Malinovsky, F. G. (2016). Understanding CrRLK1L function: cell walls and growth control. *Trends Plant Sci.* **21**, 516-527. doi:10.1016/j.tplants.2015.12.004

Ortiz-Morea, F. A., Savatin, D. V., Dejonghe, W., Kumar, R., Luo, Y., Adamowski, M., Van den Begin, J., Dressano, K., Pereira de Oliveira, G., Zhao, X. et al. (2016). Danger-associated peptide signaling in *Arabidopsis* requires clathrin. *Proc. Natl. Acad. Sci. USA* **113**, 11028-11033. doi:10.1073/pnas.1605588113

Páli, T., Dixon, N., Kee, T. P. and Marsh, D. (2004). Incorporation of the V-ATPase inhibitors concanamycin and indole pentadiene in lipid membranes. Spin-label EPR studies. *Biochim. Biophys. Acta* **1663**, 14-18. doi:10.1016/j.bbamem.2004.03.003

Park, Y., Xu, Z.-Y., Kim, S. Y., Lee, J., Choi, B., Kim, H., Sim, H.-J. and Hwang, I. (2016). Spatial regulation of ABCG25, an ABA exporter, is an important component of the mechanism controlling cellular ABA levels. *Plant Cell* **28**, 2528-2544. doi:10.1105/tpc.16.00359

Pearce, G., Moura, D. S., Stratmann, J. and Ryan, C. A.Jr. (2001). RALF, a 5-kDa ubiquitous polypeptide in plants, arrests root growth and development. *Proc. Natl. Acad. Sci. USA* **98**, 12843-12847. doi:10.1073/pnas.201416998

Ritzenthaler, C., Nebenführ, A., Movafeghi, A., Stussi-Garaud, C., Behnia, L., Pimpl, P., Staehelin, L. A. and Robinson, D. G. (2002). Reevaluation of the effects of brefeldin A on plant cells using tobacco Bright Yellow 2 cells expressing Golgi-targeted green fluorescent protein and COPI antisera. *Plant Cell* **14**, 237-261. doi:10.1105/tpc.010237

Schlessinger, J. (2002). Ligand-induced, receptor-mediated dimerization and activation of EGF receptor. *Cell* **110**, 669-672. doi:10.1016/S0092-8674(02)00966-2

Schulze-Muth, P., Irmler, S., Schröder, G. and Schröder, J. (1996). Novel type of receptor-like protein kinase from a higher plant (*Catharanthus roseus*). cDNA, gene, intramolecular autophosphorylation, and identification of a threonine important for auto- and substrate phosphorylation. *J. Biol. Chem.* **271**, 26684-26689. doi:10.1074/jbc.271.43.26684

Spallek, T., Beck, M., Ben Khaled, S., Salomon, S., Bourdais, G., Schellmann, S. and Robatzek, S. (2013). ESCRT-I mediates FLS2 endosomal sorting and plant immunity. *PLoS Genet.* **9**, e1004035. doi:10.1371/journal.pgen.1004035

Stegmann, M., Monaghan, J., Smakowska-Luzan, E., Rovenich, H., Lehner, A., Holton, N., Belkhadir, Y. and Zipfel, C. (2017). The receptor kinase FER is a RALF-regulated scaffold controlling plant immune signaling. *Science* **355**, 287-289. doi:10.1126/science.aal2541

Tse, Y. C., Lam, S. K. and Jiang, L. (2007). Enigmatic brefeldin a. *Plant Signal. Behav.* **2**, 199-202. doi:10.4161/psb.2.3.3613

Wang, C., Yan, X., Chen, Q., Jiang, N., Fu, W., Ma, B., Liu, J., Li, C., Bednarek, S. Y. and Pan, J. (2013a). Clathrin light chains regulate clathrin-mediated trafficking, auxin signaling, and development in *Arabidopsis*. *Plant Cell* **25**, 499-516. doi:10.1105/tpc.112.108373

Wang, Q., Zhao, Y., Luo, W., Li, R., He, Q., Fang, X., Michele, R. D., Ast, C., von Wiren, N. and Lin, J. (2013b). Single-particle analysis reveals shutoff control of the *Arabidopsis* ammonium transporter AMT1;3 by clustering and internalization. *Proc. Natl. Acad. Sci. USA* **110**, 13204-13209. doi:10.1073/pnas.1301160110

Wang, L., Li, H., Lv, X., Chen, T., Li, R., Xue, Y., Jiang, J., Jin, B., Baluška, F., Šamaj, J. et al. (2015). Spatiotemporal dynamics of the BRI1 receptor and its regulation by membrane microdomains in living *Arabidopsis* Cells. *Mol. Plant* **8**, 1334-1349. doi:10.1016/j.molp.2015.04.005

Xiao, Y., Stegmann, M., Han, Z., DeFalco, T. A., Parys, K., Xu, L., Belkhadir, Y., Zipfel, C. and Chai, J. (2019). Mechanisms of RALF peptide perception by a heterotypic receptor complex. *Nature* **572**, 270-274. doi:10.1038/s41586-019-1409-7

Xue, Y., Xing, J., Wan, Y., Lv, X., Fan, L., Zhang, Y., Song, K., Wang, L., Wang, X., Deng, X. et al. (2018). *Arabidopsis* blue light receptor phototropin 1 undergoes blue light-induced activation in membrane microdomains. *Mol. Plant* **11**, 846-859. doi:10.1016/j.molp.2018.04.003

Yu, F., Qian, L., Nibau, C., Duan, Q., Kita, D., Levasseur, K., Li, X., Lu, C., Li, H., Hou, C. et al. (2012). FERONIA receptor kinase pathway suppresses abscisic acid signaling in *Arabidopsis* by activating ABI2 phosphatase. *Proc. Natl. Acad. Sci. USA* **109**, 14693-14698. doi:10.1073/pnas.1212547109

Yu, M., Liu, H., Dong, Z., Xiao, J., Su, B., Fan, L., Komis, G., Šamaj, J., Lin, J. and Li, R. (2017). The dynamics and endocytosis of Flot1 protein in response to flg22 in *Arabidopsis*. *J. Plant Physiol.* **215**, 73-84. doi:10.1016/j.jplph.2017.05.010

Zhao, C., Zayed, O., Yu, Z., Jiang, W., Zhu, P., Hsu, C.-C., Zhang, L., Tao, W. A., Lozano-Durán, R. and Zhu, J.-K. (2018). Leucine-rich repeat extensin proteins regulate plant salt tolerance in *Arabidopsis*. *Proc. Natl. Acad. Sci. USA* **115**, 13123-13128. doi:10.1073/pnas.1816991115